Applied Thermal Engineering 100 (2016) 753–761

Contents lists available at ScienceDirect

Applied Thermal Engineering

journal homepage: www.elsevier.com/locate/apthermeng

Research Paper

A thermocline thermal energy storage system with filler materials for concentrated solar power plants: Experimental data and numerical model sensitivity to different experimental tank scales

J.-F. Hoffmann [a,b,c,*], T. Fasquelle [a], V. Goetz [a], X. Py [a]

[a] PROMES-CNRS UPR-8521 Laboratory, University of Perpignan Via Domitia, Rambla de la Thermodynamique, Tecnosud, 66100 Perpignan, France
[b] AQYLON, 46-48 rue Renée-Clair, 75892 Paris, France
[c] EDF – R&D, MFEE – Nouvelles Filières de Production et Thermochimie, 6 quai Watier, 78401 Chatou, France

ARTICLE INFO

Article history:
Received 30 September 2015
Accepted 22 January 2016
Available online 23 February 2016

Keywords:
Concentrated solar power (CSP)
Thermal energy storage (TES)
Thermocline
Numerical modeling

ABSTRACT

Thermocline thermal energy storage is one of the most promising, cost-effective solutions in improving concentrated solar power plant capacity factor. However, this thermal energy storage needs to be well understood; for this reason, the PROMES-CNRS laboratory built a laboratory-scale experiment. The experiment comprises a thermocline thermal energy storage tank fitted with an oil loop to heat and cool down the thermal oil flowing through the tank. The present study compares experimental results coming from the laboratory experiment but also from two large scale industrial storages already presented in the literature, with two numerical models. The 1D-1P model considers a homogeneous medium that flows through the tank, while the second one (1D-2P) distinguishes between the solid continuous medium and the fluid flowing through the void fraction. The 1D-1P model showed close agreement with experimental results when compared with industrial-size tanks, but differed markedly in the case of laboratory-scale ones. The results show that the 1D-2P model is more accurate, especially for small-size tanks. Particular attention has been paid to the tank wall and to heat losses, which have a direct influence on the outlet temperature, especially for laboratory scale tanks. With these considerations, the numerical 1D-2P model can predict the thermocline behavior with accuracy, without parameter fitting process and without a high computation time.

© 2016 Elsevier Ltd. All rights reserved.

1. Introduction

Energy supply has always been a major issue, all the more so now that fossil fuels are becoming increasingly scarce, and with mounting concerns about global warming. One solution that has emerged is the development of renewable energies. Renewable energies are theoretically inexhaustible, so renewable energies can supply the global population for at least a very long time. Concentrated solar power is one of the most promising renewable energy technologies, since solar radiation is available worldwide, and thanks to thermal energy storage [1]. Unlike photovoltaics, which produce electricity directly from sunlight, concentrated solar power first produces heat, and this heat is then used to drive a Rankine power cycle. Since thermal energy is easy to store, it is theoretically possible to overcome problems of poor weather, generate electricity at a constant power and increase plant capacity factor [2].

Usually, concentrated solar power plants use a two-tank system to store energy. When the solar resource exceeds the power block needs, a part of the heat transfer fluid, generally a synthetic oil, is diverted into a heat exchanger in which it heats another fluid, generally a molten salt. The latter is then stored in a tank called the hot tank. When there is a need for more energy than the solar radiation can provide, because of clouds or low sun elevation, the thermal energy storage fluid gives back the energy stored. To do so, it flows through the same heat exchanger, and then is stored in another tank called the cold tank. This solution is almost always chosen [3] because it is effective and easy to handle. However, it is very expensive; thermal energy storage may exceed 20% of the cost of whole solar power plant [4,5].

One way to reduce costs is to use a single tank, in which hot fluid at the top and cold fluid at the bottom are separated by the clever use of buoyancy forces [6]. As a result, a thermal gradient called a thermocline occurs between the two zones. In order to further reduce the cost of the storage component, it is possible to add low-cost solid filler materials to the tank. Thus, up to 80% of the costly fluid can be replaced, without causing any drop in energy storage efficiency [7]. Nevertheless, because of the thermal gradient, a part of the energy stored is at a lower temperature than the required working point of the power block. As a result, it is not possible to give back all the energy stored. Also, the thermocline size expands over time

* Corresponding author. Tel.: +(33) 4 68 68 22 15; fax: 33 (0)4 68 68 22 13.
E-mail address: jean-francois.hoffmann@promes.cnrs.fr (J.-F. Hoffmann).

http://dx.doi.org/10.1016/j.applthermaleng.2016.01.110
1359-4311/© 2016 Elsevier Ltd. All rights reserved.

[7,8]. A thorough understanding of the system is therefore needed to use this type of technology.

Numerical modeling helps to understand thermocline tank behavior and can provide solutions and strategies to increase thermal storage efficiency. Several kinds of numerical models have been developed so far. Some consider the fluid and solid temperatures to be equal and use a single-phase model of the tank. Two-phase models were introduced by Schumann in 1929 [9] and make a distinction between the solid temperature and the fluid temperature. In this case the two systems exchange energy as described by a convective heat transfer coefficient. Beasleyt and Clark published a list of all the single-phase and two-phase models in 1984 [10]. It shows that there is a general preference for Schumann-like models. In 2010, Singh et al. presented an extensive review on the research done on packed beds [11]. Since then, two-dimensional models [12,13] and even three-dimensional models [14] have been developed. Continuity and momentum equations have sometimes been added in order to describe the velocity and pressure fields within the tank. These more accurate models account for heat loss effects, wall influence on the thermocline, and fluid flow discrepancies along the tank. They also permit detailed parametric studies of the tank [7,15–21]. Non-homogeneous models have also been created to investigate the influence of particle size and characteristics [22].

Thus, today, there is a broad diversity of thermal balance formulations corresponding to different levels of detail and accuracy and also widely different calculation times. As a consequence, the trade-off between these conflicting requirements is currently being studied.

To achieve higher computation speed, Powell and Edgar [23] suggested an adaptive grid to follow the thermocline movement and focus on the thermal gradient details while reducing the grid size of the isothermal zone. Some authors, e.g. Bayón and Rojas [24], also opted for a return to the single-phase model. Some authors developed solutions by the method of characteristics, which can resolve the one-dimensional equation system without an iterative method [25,26]. A faster but fuzzier solution is to predict thermocline behavior by means of analytical functions that need no mesh-grids at all [8,27].

The present study set out to demonstrate that a one-dimensional numerical model would be sufficient to predict the general behavior of the thermocline, with an appropriate level of accuracy and independently of the tank size. To this end, the results obtained from our home-made numerical model were compared with experimental data from three different tank scales: (i) Solar One test results [28], (ii) Pacheco et al.'s pilot scale thermocline tank results [6] and (iii) results from our own laboratory-scale experiment.

2. Model descriptions

Two numerical models were developed in this work: a one-phase one-dimensional model (1D-1P) and a two-phase one-dimensional model (1D-2P). These have, however, many similarities that will be presented in this section.

The tank is considered as a perfect vertical standing cylinder that contains a solid packed bed with fluid flowing through the void fraction. No diffusers (or distributors) in the tank top and bottom are included in the models. The fluid flow inside the tank is considered uniform and one-dimensional (in the tank axis direction (x)). Continuity and momentum equations are not resolved; the numerical model only enables a tank thermal behavior evaluation. The diameter of the spherical elements is small enough to consider a homogenous temperature inside them. The Biot number (Bi) of the solid particles does not exceed the conventional limitation (Bi < 0.1) [29]. The limitation by heat transfer conduction inside the particles is therefore considered negligible. The rock bed is not modeled as independent particles, and the solid filler is considered as a continuous, homogenous and isotropic porous medium [13,29]. Radial temperature discrepancies are assumed to be negligible. With all these assumptions, the numerical model can be one-dimensional.

The tank wall and the heat losses are taken into account in both models (1D-1P and 1D-2P). The first model 1D-1P that was developed considers the fluid, the solid and the wall temperatures to be the same, so it deals with a single-phase system. The wall is thus considered by means of effective parameters. The second model 1D-2P considers the solid and the fluid temperatures to be different, so it deals with a two-phase system in the tank. The wall is considered as a third component.

Finally, in both models, thermal and thermo-physical properties of the heat transfer fluid (HTF) are dependent on the temperature. Actually less sensitive to temperature variations, the thermal and thermo-physical properties of thermal energy storage material (TESM) are considered independent of the temperature.

2.1. Development of a single-phase model (1D-1P)

The one-phase or dispersion model consists only of the development of a single thermal balance equation, which must be representative of the different components of the tank. The thermal energy storage system is considered as a single effective storage medium inside the tank. In this type of model, since the heat transfer limitation between fluid and solid are not taken into account, the packed bed must have a low Biot number. The temperatures of the solid and the fluid phases are the same regardless of the time. The 1D-1P model leads the calculation of an equivalent medium temperature T and the thermocline evolution over the time t and along the tank height x. The numerical model is governed by the following equation:

$$(\rho C_p)_{eff}\frac{\partial T}{\partial t}+\varepsilon(\rho C_p)_{eff}\,u\frac{\partial T}{\partial x}=k_{eff}\frac{\partial^2 T}{\partial x^2}+h_{ext}\frac{A_{w\leftrightarrow ext}}{V_{tot}}(T-T_{ext}) \tag{1}$$

The fluid velocity inside the filler bed is defined in Eq. (2). It is calculated from the mass flow rate data, the fluid density and the cross-sectional area of the tank:

$$u=\frac{\dot{m}}{\rho_f\left(\varepsilon\pi\left(\frac{D}{2}\right)^2\right)} \tag{2}$$

The effective volumetric heat capacity $(\rho C_p)_{eff}$ takes into account the void fraction or porosity ε and the thermal and thermo-physical properties of the fluid and of the solid medium. In the present study, according to experimental tank scales, the volumetric heat capacity of the metal wall is added to the effective parameter (Eq. 3):

$$(\rho C_p)_{eff}=\varepsilon(\rho C_p)_f+(1-\varepsilon)(\rho C_p)_s+\frac{V_w}{V_f+V_s}(\rho C_p)_w \tag{3}$$

An effective conductivity. It comprises the fluid, the solid and the wall conductivities, and takes into account the different proportions (Eq. 4):

$$k_{eff}=\varepsilon k_f+(1-\varepsilon)k_s+\frac{V_w}{V_f+V_s}k_w \tag{4}$$

All these assumptions make this type of numerical model faster than the two-phase models, because they consider the whole tank as one system.

To determine the heat losses from the present study experimental tank (description in Section 3.1), two tests were carried out.

First, oil at high temperature (TH) was sent with a constant flow into the tank. Outlet temperature at equilibrium was measured (205 °C). The thermal resistance at high temperature was thus calculated ($R_{th,TH} = 0.65$ K W^{-1}). The same test was performed at low temperature TL ($R_{th,TL} = 0.83$ K W^{-1}). A linear interpolation enabled to approximate the thermal resistance values for intermediate temperatures. Regarding the two other tanks (description in section 3.2), thermal heat losses were calculated with a global heat transfer coefficient. The thermal resistance was determined, thanks to the following equation:

$$R_{th} = \frac{1}{h_{ext} \cdot 2 \cdot \pi \cdot (r_{w+ins}) \cdot H} = \frac{\ln\left(\frac{r_{w+ins}}{r_w}\right)}{2 \cdot \pi \cdot \lambda_{ins} \cdot H} + \frac{1}{h_{air} \cdot 2 \cdot \pi \cdot (r_{w+ins}) \cdot H} \quad (5)$$

The forced convection correlation for laminar incompressible flow over a flat surface was determined, thanks to the following equation:

$$h_{air} = \frac{0.664 \mathrm{Re}_{air}^{0.5} \mathrm{Pr}_{air}^{0.5} k_{air}}{H} \quad (6)$$

2.2. Development of a dual-phase model (1D-2P)

The dual-phase one-dimensional model treats two distinct systems inside the tank: the fluid 'f', the solid 's' and one additional system composed by the wall 'w'. The fluid and the solid were considered as continuous media that exchange heat with each other. The wall exchanges heat with the fluid and the solid on its inner side, and with the surroundings on its outer side. Therefore, the three governing equations of the system are:

For the fluid:

$$\varepsilon(\rho C_p)_f \left(\frac{\partial T_f}{\partial t} + u\frac{\partial T_f}{\partial x}\right) = k_{feff}\frac{\partial^2 T_f}{\partial x^2} + h_V(T_s - T_f) + h_w\frac{A_{f\leftrightarrow w}}{V_f}(T_w - T_f) \quad (7)$$

For the solid:

$$(1-\varepsilon)(\rho C_p)_s \frac{\partial T_s}{\partial t} = k_{seff}\frac{\partial^2 T_s}{\partial x^2} + h_V(T_f - T_s) + h_w\frac{A_{s\leftrightarrow w}}{V_s}(T_w - T_s) \quad (8)$$

For the wall:

$$(\rho C_p)_w \frac{\partial T_w}{\partial t} = k_w\frac{\partial^2 T_w}{\partial x^2} + h_w\left[\frac{A_{f\leftrightarrow w}}{V_w}(T_f - T_w) + \frac{A_{s\leftrightarrow w}}{V_w}(T_s - T_w)\right] + h_{ext}\frac{A_{w\leftrightarrow ext}}{V_w}(T_w - T_{ext}) \quad (9)$$

The fluid velocity, which is needed to solve the fluid governing equation, is given in Eq. (2). The effective thermal conductivities of HTF and solid fillers, k_{feff} and k_{seff}, are the key thermo-physical properties to estimate the heat transfer inside the packed bed system. Numerous effective thermal conductivities have been set up over the past years. Xu et al. studied the impact of different effective thermal conductivities [13] on the thermal gradient and found few differences between the results. In this work, the simplest correlations were selected to estimate these two effective parameters. They are introduced in Eq. (10) [13]:

$$k_{feff} = \varepsilon k_f; \quad k_{seff} = (1-\varepsilon)k_s \quad (10)$$

The interstitial heat transfer coefficient between fluid and solid is calculated with the following equation of Xu et al. [13].

$$h_V = \frac{6(1-\varepsilon)k_{feff}\left[2 + 1.1\mathrm{Re}_p^{0.6}\mathrm{Pr}^{1/3}\right]}{d_p^2} \quad (11)$$

The related Prandtl number and Reynolds number for the interstitial heat transfer coefficient are:

$$\mathrm{Pr} = \frac{C_{pf}\mu_f}{k_f}, \quad \mathrm{Re}_p = \frac{\rho_f d_p u}{\mu_f} \quad (12)$$

Eq. (13) suggests an approximation for the heat transfer coefficient between the tank inside and the wall with the following equation of Ismail and Stuginsky [30].

$$h_w = \frac{k_f}{d_p}\left(2.576 \cdot \mathrm{Re}^{1/3} \cdot \mathrm{Pr}^{1/3} + 0.0936 \cdot \mathrm{Re}^{0.8} \cdot \mathrm{Pr}^{0.4}\right) \quad (13)$$

The heat loss coefficient is determined on the same assumptions as for the first numerical model.

Eqs. (7)–(13) correspond to the two-phase one-dimensional model. It is considered more accurate than the previous model, but loses some computation speed.

2.3. Initial and boundary conditions

The initial conditions for the discharge are:

$$T_f(t=0) = T_s(t=0) = T_w(t=0) = T_{\exp}(t=0) \quad (14)$$

Regarding the boundary conditions during a discharge, since the numerical models consider one-dimensional media, there is only one on the bottom of the tank and one on the top.

The cold heat transfer fluid enters the tank from the bottom, which means an adiabatic condition for the solid and for the wall and inlet temperature and velocity for the fluid conditions.

$$T_f(x=0) = T_L \quad (15)$$

$$\frac{\partial T_s(x=0)}{\partial x} = \frac{\partial T_w(x=0)}{\partial x} = 0 \quad (16)$$

Hot heat transfer fluid leaves the tank, which means there is an adiabatic condition for the fluid and for the solid.

$$\frac{\partial T_f(x=H)}{\partial x} = \frac{\partial T_s(x=H)}{\partial x} = \frac{\partial T_w(x=H)}{\partial x} = 0 \quad (17)$$

2.4. Numerical method

The above equation systems were numerically solved by means of a finite difference method, with a second order central differencing scheme for the second order derivative terms, a central differencing scheme for the first order derivative terms and an implicit scheme for the time discretization. The solution is found via an iterative method in order to find the one or the three temperature vectors (fluid, solid and wall) at the same time, for each time step, and with a 10^{-4} convergence criterion. For the sake of computation speed, the fluid properties are updated only every 4 minutes of simulated time. This interval corresponds to a maximum fluid temperature difference of 6.9 °C, with an average deviation of 0.7 °C. Finally, this means that there is a maximum error of 3.6% in fluid viscosity, and a maximum error of 0.3% in the other fluid property values. The numerical model was totally written and computed in Matlab® commercial software. Because a computation speed comparison was made, we give the computer technical specifications: OS X Yosemite version 10.10.3, 2.3 GHz Intel Core i7 processor, memory 16 Go 1600 MHz DDR3, and 256 Gb SATA SSD hard disk.

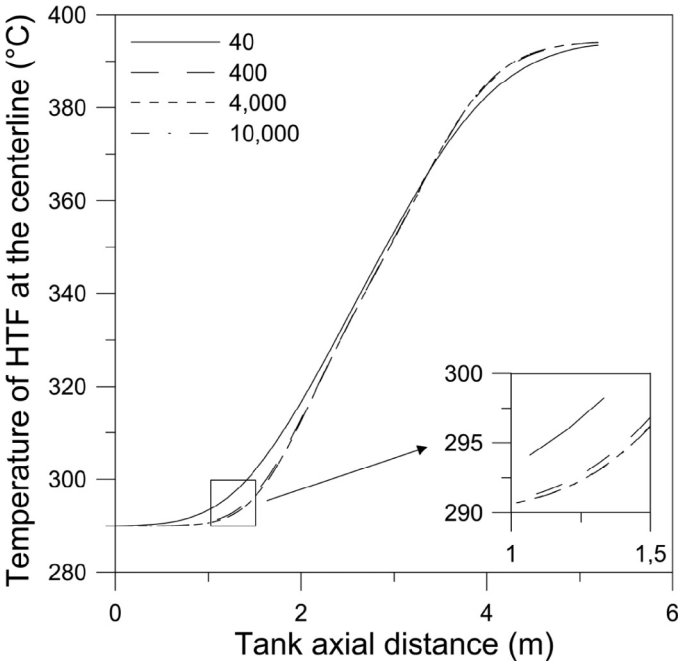

Fig. 1. Temperature profile at the centerline with different grid size for the 1D-2P numerical model.

2.5. Sensitivity of the grid size

Numerical models are sensitive to the grid size, i.e. the number of control volumes. Powell and Edgar showed that an insufficient number of control volumes can lead to numerical diffusion [23]. We therefore investigated the influence of grid size on the results from our numerical model (Fig. 1). We compared temperature profiles along the tank axis for numerous grid sizes, from 40 to 10,000 control volumes. Above 4,000 control volumes, the temperature differences were negligible.

3. Experimental

3.1. The present study experimental set-up

The laboratory-scale experiment built at the PROMES-CNRS laboratory comprises a thermocline thermal energy storage tank fitted with an oil loop to heat and cool down the thermal oil flowing through the tank. The experiment structure is depicted in Fig. 2, and all its characteristics are listed in Table 1. The tank, of storage capacity 8.3 kWh, was filled with quartzite rock with an average equivalent particle diameter of 0.04 m. The void fraction or porosity of the tank (0.41) was determined from the solid mass and density. The mass of TESM was 325 kg. The tank contained two buffer sections to homogenize the downward or upward fluid flow. The thermal energy storage section was 1.8 m high with a diameter of 0.4 m. It was insulated with 20 cm of rock wool covered with aluminum foil. To facilitate the tank filling and emptying, it was divided into three parts held together by flanges. The total mass of steel was approximately 150 kg. A series of 32 thermocouples inserted along the tank height was used to study the temperature profile time course. Several thermocouples were also used to evaluate the radial thermal gradient and the difference between the oil and the solid temperatures. The oil loop heated the oil with heaters of total thermal power 9 kW. It was possible to separately heat an amount of oil equivalent to the tank oil volume. Hot oil could then be sent to the tank to store energy. Oil cooling during a discharge was possible,

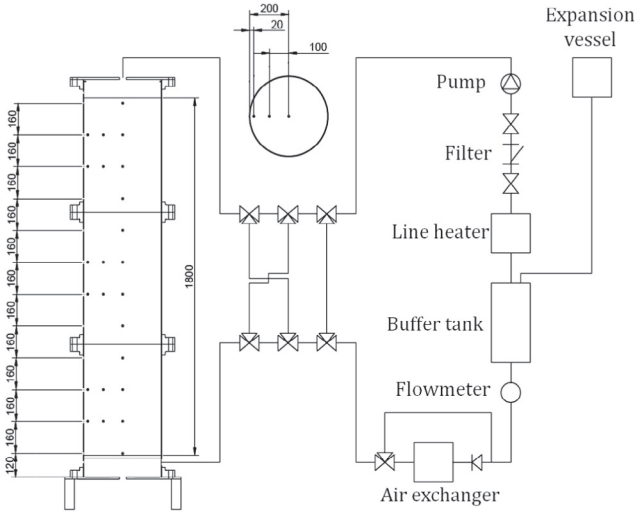

Fig. 2. The present study demonstrator illustrated with the temperature measurement positions and each mechanism.

thanks to an air heat exchanger of capacity 25 kW. The flow was measured with a Brooks MT 3809 flow meter calibrated with respect to the temperature of the fluid flowing through, to an accuracy of ± 10%. The discharge process started when the tank was almost entirely at 210 °C, by sending oil at 160 °C to the bottom of the tank and with a mass flow of 1.91 10^{-2} kg s^{-1}.

3.2. Sandia National Laboratory (S.N.L.) and Solar One power plant experiments

Sandia National Laboratory constructed a thermocline thermal energy storage tank of capacity 2.3 MWh_T. The S.N.L. tank was 6.1 m high and 1.5 m in radius. It ran with solar salt and was partially filled with a mixture of quartzite rock and silica sand. The bed porosity was reported to be 0.22 due to the sand, which lowered the void fraction. The bed height, with this porosity, measured 5.2 m. The hot and cold temperatures of the experiment were 395 °C and 290 °C respectively.

S.N.L. published experimental data from this tank. These data represented temperature curves during 2 hours of discharge [6]. The authors did not report either molten salt flow rates or initial temperature condition. However, these data are necessary to perform a numerical simulation of the thermocline tank. Some authors have

Table 1
Main characteristic for the present study demonstrator, Sandia Laboratory and Solar One pilots.

Parameter	Promes-CNRS Laboratory demonstrator	Sandia Laboratory pilot [6]	Solar One pilot [28,31]
Energy	8.3 kWh_T	2.3 MWh_T	170 MWh_T
HTF	Rapeseed oil	Solar salt	Caloria HT 43
TESM	Quartzite rock	Quartzite rock and sand	Granite rock and sand
Discharge time, t	3 h	3 h	8 h
Tank height, H	1.8 m	6.1 m	12 m
Tank diameter, D	0.4 m	3 m	18.2 m
Volume, V	0.25 m^3	42 m^3	3122 m^3
Porosity, ε	0.41	0.22	0.22
Diameter particle, d_p	40 10^{-3} m	19.1 10^{-3} m	4.6 10^{-3} m
HTF mass flow rate, $\dot{m}$	1.9 10^{-2} kg s^{-1}	5.46 kg s^{-1}	23 kg s^{-1}
T_H	210 °C	395.9 °C	295.5 °C
T_L	160 °C	289 °C	179.2 °C

Table 2
Thermal and thermo-physical properties of the HTF.

Rapeseed oil	ρ_f	kg m^{-3}	928.19 – 0.6691 T
	C_{pf}	J kg^{-1} K^{-1}	$(1.621\times10^{-9}\,T^4 - 8.735\times10^{-7}\,T^3 + 14.933\times10^{-5}\,T^2 - 5.976\times10^{-3}\,T + 2.0985)\times1000$
	k_f	W m^{-1} K^{-1}	$2.00\times10^{-7}\,T^2 + 1.714\times10^{-4}\,T + 0{,}1698$
	μ_f	Pa s	$(39\,498\,T^{-1.764})/1000$
Caloria HT 43 [33,34]	ρ_f	kg m^{-3}	871.1 – 0.713 T
	C_{pf}	J kg^{-1} K^{-1}	1836.8 + 3.456 T
	k_f	W m^{-1} K^{-1}	0.125 + 0.00014 T
	μ_f	Pa s	$72.159\,T^{-2.096}$
Solar salt [32]	ρ_f,	kg m^{-3}	2090 – 0.636 T
	C_{pf}	J kg^{-1} K^{-1}	1443 + 0.172 T
	k_f	W m^{-1} K^{-1}	0.443 + 0.00019 T
	μ_f	Pa s	$(22.174 - 0.12\,T + 2.281\times10^{-4}\,T^2 - 1.474\times10^{-7}\,T^3)/1000$

estimated that the cold molten salt entered the packed bed at a velocity of 4.36 10^{-4} m s^{-1} [29,32]. In the present study, the first measured temperature profile was used as the initial temperature condition for the numerical models.

A thermocline tank was used in the Solar One pilot plant, and the stored energy was reported to be 170 MWh_T [28,31]. The thermal energy storage system operated from 1982 to 1986. It supplied 8 hours of additional electrical production to the power plant and showed a very thin thermocline layer. The tank was composed of a carbon steel wall with a diameter of 18.2 m and a height of 12 m. The wall thickness was 2.89 cm at the bottom and 0.79 cm near the top. It was the only industrial-scale thermal energy storage of its kind. It ran with Caloria HT 43 synthetic oil working between 179 °C and 295 °C. The filler bed was a mixture of granite rock and sand, and the average diameter was 4.6×10^{-3} m, with a void fraction of 0.22. In the present study, the velocity of the cold oil entering the packed bed was estimated from different Sandia reports [28,31]. The first measured temperature profile was also used as the initial temperature condition.

The characteristics of the two experiments are listed in Table 1.

4. Results and discussion

The objective of the present study was to find a numerical model able to predict the thermocline behavior inside any tank, regardless of its scale, and with a high computation speed. The two numerical models were first compared. We then used the better one to investigate heat loss and wall implementation.

4.1. Comparison of the two numerical model results

The thermo-physical properties of the working fluids and the filler material are listed in Tables 2 and 3, respectively. As stated above, the initial states of the S.N.L. and Solar One were set to the first known temperature profiles. The initial state of our experiment also matched the first experimental curve and corresponded to a tank almost fully loaded.

Temperature profiles inside the tanks are presented in Figs. 3–5. All the results represent the temperature profiles along the tank axis during a discharge process and over time. The "sampling" time step

Table 3
Thermal and thermo-physical properties of the TESM.

Quartzite [13]	ρ_s	kg m^{-3}	2500
	C_{ps}	J kg^{-1} K^{-1}	830
	k_s	W m^{-1} K^{-1}	5.69
Granit rock and sand [24]	ρ_s	kg m^{-3}	2643
	C_{ps}	J kg^{-1} K^{-1}	1020
	k_s	W m^{-1} K^{-1}	2.2

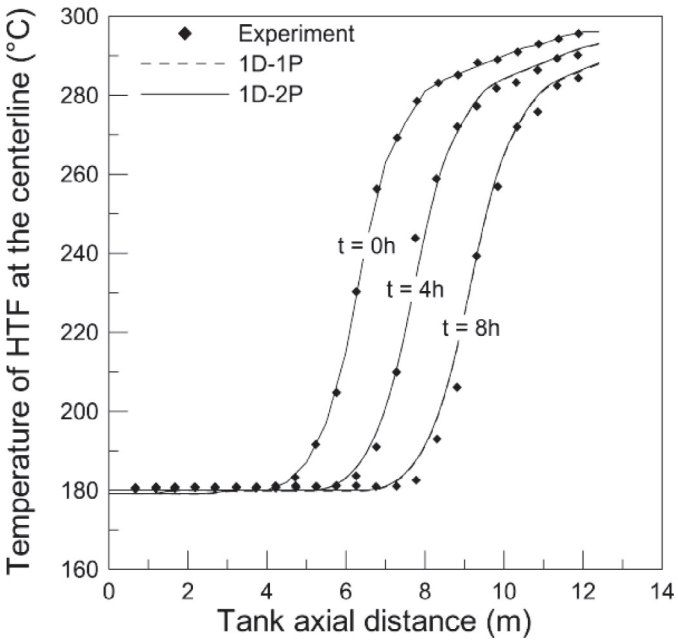

Fig. 3. Comparison of the 1D-1P numerical model results, the 1D-2P numerical model results and the experimental data from Solar One pilot.

was 0.5 h for S.N.L. and for our tank results, and 4 h for Solar One results. Experimental results are represented by dots, and simulated profiles by lines. In order to differentiate between the two numerical model results, 1D-1P is represented by dashed lines, while the 1D-2P is represented by continuous lines.

As expected, computation for the single-phase model was 6 times faster than for the two-phase model, with a total computation time of 4516 seconds for the 1D-2P model for S.N.L. For the Solar One and S.N.L. temperature profile results, Figs. 3 and 4 show no significant differences between the three sets of results (experimental, 1D-1P model and 1D-2P model results). Hence both numerical

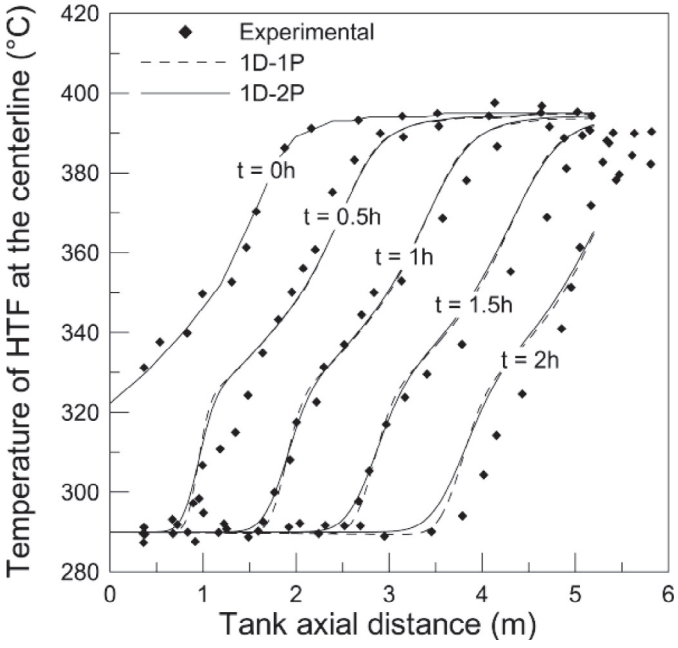

Fig. 4. Comparison of the 1D-1P numerical model results, the 1D-2P numerical model results and the experimental data from Sandia Laboratory pilot.

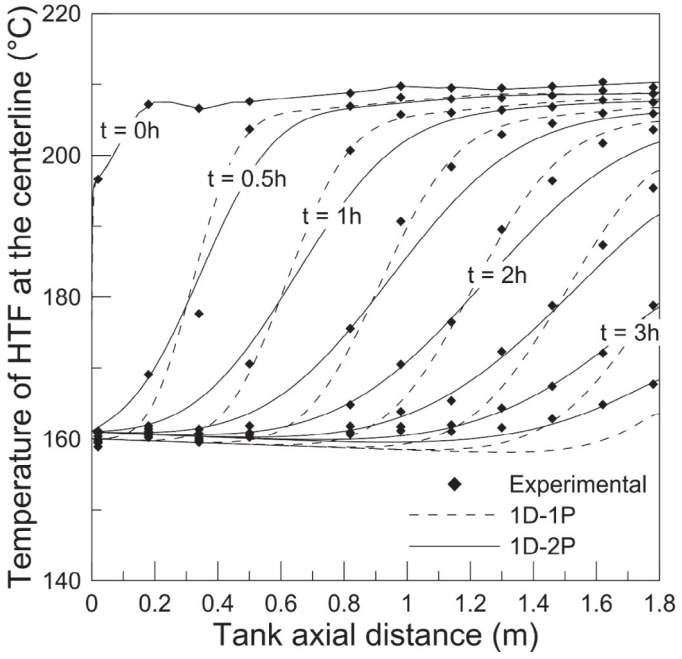

Fig. 5. Comparison of the 1D-1P numerical model results, the 1D-2P numerical model results and the experimental data from the present study laboratory demonstrator.

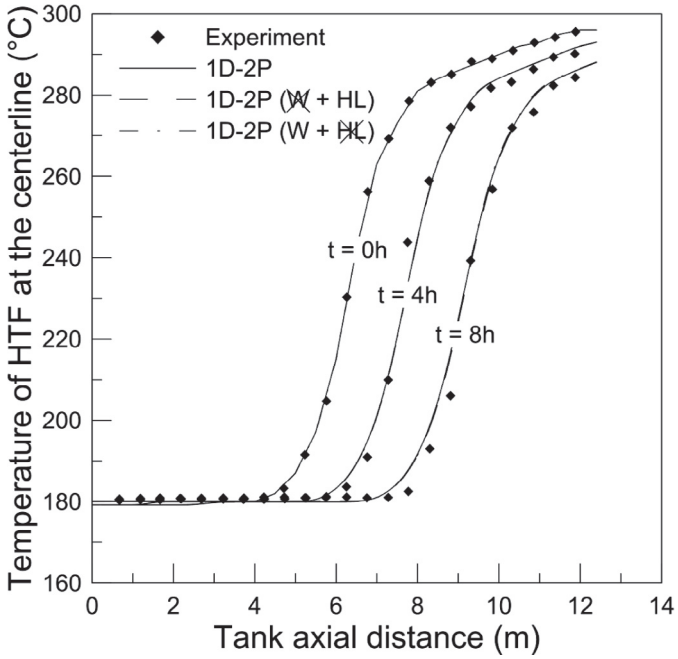

Fig. 6. Comparison of the 1D-2P numerical model results with and without wall (W) and heat losses (HL), and the experimental data from Solar One power plant thermal energy storage tank.

models appear to be in reasonable agreement with large-scale tank experimental data. It is important to keep in mind that no parameter-fitting processes were performed. However, the discrepancies were more pronounced for our experimental data (Fig. 5 and Table 4). Different errors are presented in Table 4. They have been calculated from the data of the 7 experimental temperature profiles and the corresponding simulated temperatures. The 1D-2P model gives a better representation of the system's thermal behavior. For the gradient temperature at the centerline, there was an average error of 1.75 °C for the 1D-1P model, with a maximum of 7.77 °C, while the 1D-2P model predicted it with an average error of 1.32 °C and a maximum of 6.4 °C. The limit accuracy of the 1D-1P model may be due to its inherent assumptions: the model assumes identical temperature of the fluid and the solid, at all times. This does not seem to be the case, especially in the bottom part of the tank, where cold fluid meets solid particles at high temperature. As a result, the 1D-1P model predicts a too-high fluid temperature, and the results differ from the experimental ones. For the two other experiments because their height is greater, this difference seems less pronounced. To conclude, the 1D-1P model should be used with caution, while the 1D-2P model results seem to agree with experimental behavior, independent of the tank size.

Table 4
Error between experimental gradient temperature from the present study laboratory demonstrator and numerical model $rMSE = 1/n\ \Sigma\ ((T_{exp}\text{-}T)/T_{exp})^2$.

Numerical model	Average error (°C)	Maximum error (°C)	Relative Mean Square Error (rMSE)
1D-1P	1.75	7.77	$2.1\ 10^{-4}$
1D-2P	1.32	6.40	$1.2\ 10^{-4}$
1D-2P Without W	3.58	13.77	$8.2\ 10^{-4}$
1D-2P Without HL	1.67	5.75	$1.4\ 10^{-4}$

4.2. Simplified 1D-2P models

The 1D-2P model gives good accuracy in all cases but requires much more computation time. In order to overcome this limitation that could be detrimental when tank cycling simulations are needed, two simplifications have been tested for 1D-2P model, i.e., sensitivity of the temperature profiles to heat losses and to the thermal masses corresponding to the storage wall. We assessed the impact of these two simplifications.

First, we tested the influence of the heat losses on the model's accuracy. We thus took an adiabatic numerical model, but still comprising the tank wall. Figures 6–8 show the results obtained and their comparison with the original model results. We can see that it may not always be useful to include heat losses in numerical models when working on large tanks (Figs. 6 and 7): with and without heat losses the results show a globally good agreement between numerical and experimental results for the two biggest experiments. However, in the case of our experiment (Fig. 8 and Table 4), the adiabatic model was no longer able to predict the temperature with accuracy: the average error in the predicted results was 1.67 °C. Removing the heat losses prevents a good simulation of the tank's thermal behavior in this case, since 9.5% of the energy stored was lost during the test. Regarding Solar One and Sandia National Laboratory models, it respectively represented 0.08% and 0.95% of the energy stored. The real heat losses were certainly higher but there were no available experimental data about them.

It is thus advisable to include heat losses in numerical models. But removing the tank wall to obtain a higher computation speed can be envisaged. The wall is a third system to be modeled in the 1D-2P numerical model. The 1D-2P numerical model results, with and without the wall and for the three storages (Figs. 6, 7 and 9), were compared. The heat losses, of course, were kept in the simulation. A difference of 13% was found in the computation speed. Adding the wall had practically no influence on the Solar One numerical results (Fig. 6), but had a slight influence on the S.N.L. results (Fig. 7). It had a non-negligible influence on our tank numerical results (Fig. 9 and Table 4), with an average error of 3.58 °C, and a

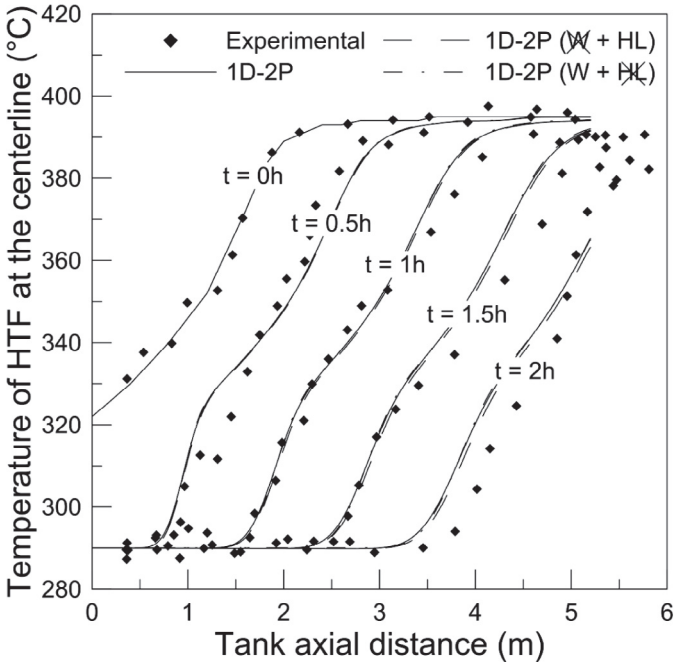

Fig. 7. Comparison of the 1D-2P numerical model results with and without wall (W) and heat losses (HL), and the experimental data from Sandia National Laboratory thermal energy storage pilot.

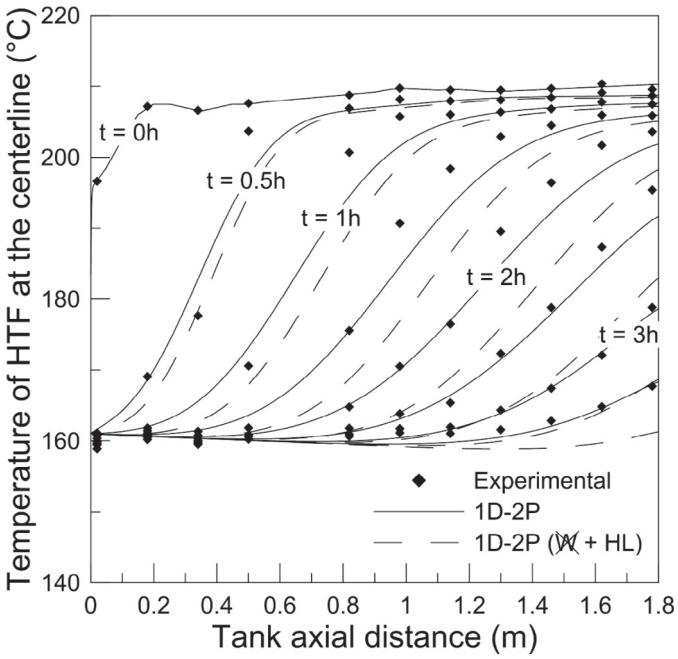

Fig. 9. Comparison of the 1D-2P numerical model results with and without tank wall, and the experimental data from the present study demonstrator.

maximum of 13.8 °C, in the predicted temperature. In our experiment, the wall with the flanges (included in the modeling by an effective wall thickness) represented 13.3% of the total thermal energy storage capacity; in the other two experiments, it respectively represented only 0.6% and 4.1%. Hence above a proportion of about 5% of the energy storage capacity, the wall needs to be included in the computation.

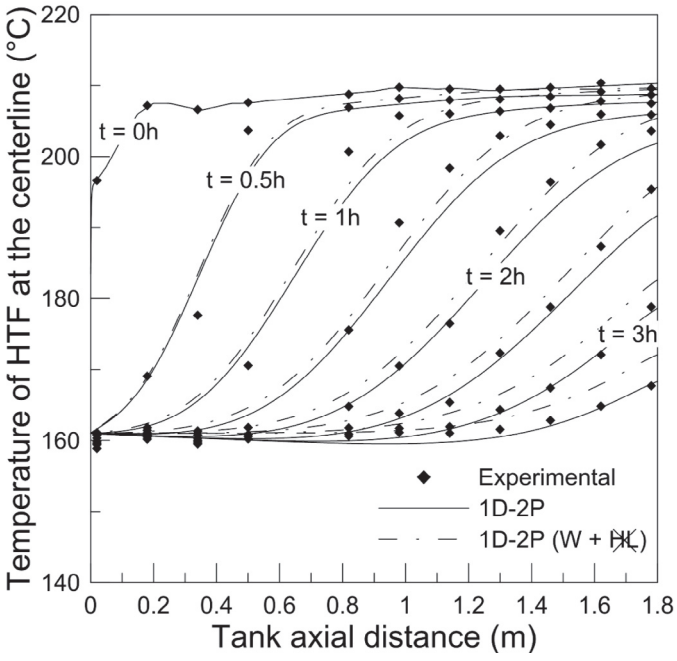

Fig. 8. Comparison of the 1D-2P numerical model results with and without heat losses (HL), and the experimental data from the present study laboratory demonstrator.

4.3. The outlet temperature criterion

Most of the available experimental data represent the global thermal gradient in the tank. The latter is therefore used to quantify the model accuracies. However, the fluid profiles is probably the most relevant criterion to characterize the working mode of the storage. It is directly connected to the thermal energy storage efficiency. It also represents the inlet temperature of the other parts of the plant (for example the power group in a concentrated solar power plant).

Hence the outlet temperature of our laboratory-scale tank was used to compare the models with each other. Results are depicted in Fig. 10 and Table 5. The 1D-1P numerical model gives a rather good estimation of the outlet temperatures. It seems to better represent them than the 1D-2P model in the beginning of the discharge but underestimated them in the end. Also, once again, the 1D-2P model is the most accurate one, with an average error of 0.93 °C in the predicted outlet temperatures and a maximum error of 3.79 °C. The 1D-2P adiabatic model (i.e. with wall and without heat losses) predicted too high outlet temperatures while the 1D-2P model without wall predicted too low temperatures.

5. Conclusion

Thermocline thermal energy storage technology can reduce concentrated solar power plant costs, but an optimal management of the storage necessitates a thorough comprehension of its behavior. To this end, many numerical models have been developed in recent years. These models are generally compared with experimental data from a very small set of instrumented tanks. However, there is a need for very fast numerical models that can predict the global thermocline behavior over time whatever the size. There is also a need for the acquisition of new experimental data to validate these models and improve the understanding and management of thermocline behavior. This work thus aimed to find the simplest but still sufficiently accurate numerical model, and to provide new thermocline thermal energy storage experimental data.

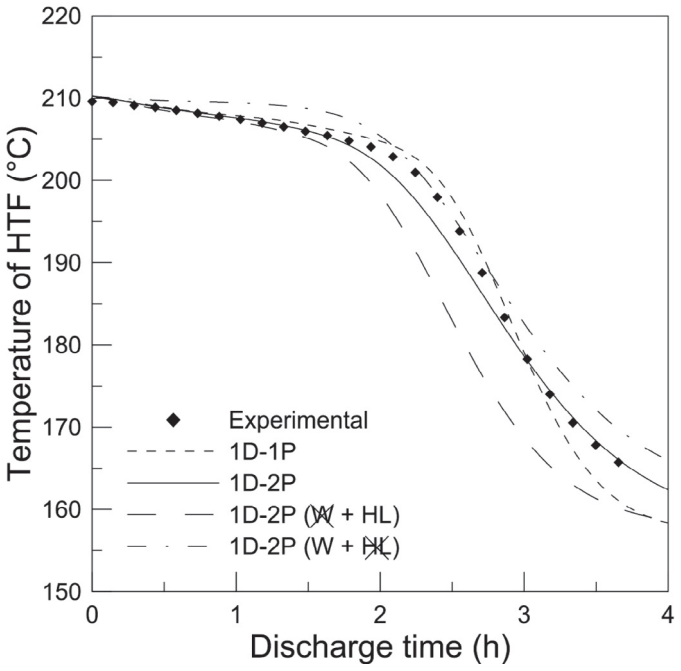

Fig. 10. Comparison of all numerical models and the experimental outlet temperature from the present study demonstrator.

A comparative study of two numerical models was performed. Both models were one-dimensional, based on the partial differential equations originating from thermal balances, and discretized with the finite difference method. Both formulations took into account the tank wall and the heat losses. The 1D-1P considers a homogeneous medium that flows through the tank, while the second one (1D-2P) distinguishes between the solid continuous medium and the fluid flowing through the void fraction. Before comparing the different results, a sensitivity analysis was performed regarding the mesh grid to be sure it did not influence the numerical results. Both models were then computed to simulate temperature profiles in three storage tanks with very different scales.

Since the 1D-1P model only considers one effective system, which integrates the fluid, the solid and the wall, it is obviously faster than the 1D-2P model. But the 1D-2P model is more accurate, especially for small-size tanks. It is therefore advisable to use such a model for reliable results.

Attempts of simplification of the 1D-2P numerical model were tested by successively removing the heat losses and the wall. We found that both the heat losses and the wall were essential for small tanks. In this case, heat losses are necessary to correctly predict the tank outlet temperature, while the tank wall may exert a non-negligible effect on the temperature profiles inside the tank. It can be considered that below 5% of the total thermal energy storage capacity, it is not useful to add the wall to the simulation.

Finally, the present study develops a thermocline thermal energy storage experiment and shows that a quite simple numerical model is able to predict experimental results over a broad range of tank scales, where an analytical model would have required parameter-fitting processes and a 3D complex model would have spent a lot of calculation time. This will enable us to perform experimental and numerical parametric studies in parallel.

Table 5
Error between experimental outlet temperature from the present study laboratory demonstrator and numerical model $rMSE = 1/n\ \Sigma\ ((T_{exp}\text{-}T)/T_{exp})^2$.

Numerical model	Average error (°C)	Maximum error (°C)	Relative Mean Square Error (rMSE)
1D-1P	1.33	4.74	$1.1\ 10^{-4}$
1D-2P	0.93	3.79	$0.6\ 10^{-4}$
1D-2P Without W	4.68	12.73	$12.4\ 10^{-4}$
1D-2P Without HL	2.11	4.52	$1.9\ 10^{-4}$

Acknowledgements

The project was supported financially by ANRT (ANRT CIFRE n° 2012/1516) for a PhD grant through a CIFRE program, AQYLON and EDF R&D.

The authors would like to thank A. Bouvier d'Acher for the demonstrator experimentation and. G. Hernandez, J.-J. Huc, and J.-M. Mancaux for their help in building the demonstrator.

Nomenclature

Dimensionless numbers

Bi	Biot number [-]
Pr	Prandtl number [-]
Re	Reynolds number [-]

Greek letters

μ	Dynamic viscosity [Pa s]
ρ	Density [kg m^{-3}]
ε	Void fraction [-]

Latin letters

$\dot{m}$	Mass flow rate [kg s^{-1}]
A	Area [m^2]
C_p	Specific heat [J kg^{-1} K^{-1}]
D	Diameter of packed bed [m]
d_p	Diameter of particles [m]
H	Height of packed bed [m]
h_{air}	Convection coefficient of air over a flat surface [W m^{-2} K^{-1}]
h_{ext}	Coefficient of global thermal losses to the environment [W m^{-2} K^{-1}]
h_v	Interstitial heat transfer coefficient [W m^{-3} K^{-1}]
h_w	Heat transfer coefficient through the wall [W m^{-2} K^{-1}]
k	Thermal conductivity [W m^{-1} K^{-1}]
R_{th}	Thermal resistance [K W^{-1}]
T	Temperature [°C]
t	Time [s]
u	Velocity [m s^{-1}]
V	Volume [m^3]
x	Axial coordinate of bed [m]

Subscripts

tot	Relative to the whole tank (fluid, solid and wall)
s↔w	Between the solid and the wall
f↔w	Between the fluid and the wall
w↔ext	Between the wall and the outside
air	Air
amb	Ambient
eff	Effective
exp	Experimentation
f	Fluid
H	High
ins	Insulation
L	Low
s	Solid
w	Wall

References

[1] D. Barlev, R. Vidu, P. Stroeve, Innovation in concentrated solar power, Sol. Energy Mater. Sol. Cells 95 (2011) 2703–2725.
[2] M. Medrano, A. Gil, I. Martorell, X. Potau, L.F. Cabeza, State of the art on high-temperature thermal energy storage for power generation. Part 2 – case studies, Renew. Sustain. Energy Rev. 14 (2010) 56–72.
[3] S. Kuravi, J. Trahan, D.Y. Goswami, M.M. Rahman, E.K. Stefanakos, Thermal energy storage technologies and systems for concentrating solar power plants, Progr. Energy Combus. Science 39 (2013) 285–319.
[4] U. Herrmann, B. Kelly, H. Price, Two-tank molten salt storage for parabolic trough solar power plants, Energy 29 (2004) 883–893.
[5] G. Angelini, A. Lucchini, G. Manzolini, Comparison of thermocline molten salt storage performances to commercial two-tank configuration, Energy Procedia 49 (2013) 694–704.
[6] J.E. Pacheco, S.K. Showalter, W.J. Kolb, Development of a molten-Salt thermocline thermal storage system for parabolic trough plants, J. Solar Energy Eng. 124 (2002) 153–159.
[7] C. Xu, Z. Wang, Y. He, X. Li, F. Bai, Parametric study and standby behavior of a packed-bed molten salt thermocline thermal storage system, Renew. Energy 48 (2012) 1–9.
[8] R. Bayón, E. Rivas, E. Rojas, Study of thermocline tank Performance in dynamic processes and stand-by periods with an analytical function, Energy Procedia 49 (2014) 725–734.
[9] T.E.W. Schumann, Heat transfer: a liquid flowing through a porous prism, J. Franklin Inst. 208 (1929) 405–416.
[10] D.E. Beasleyt, J.A. Clark, Transient response of a packed bed for thermal energy storage, Int. J. Heat Mass Transf. 27 (1984) 1659–1669.
[11] H. Singh, R.P. Saini, J.S. Saini, A review on packed bed solar energy storage systems, Renew. Sustain. Energy Rev. 14 (2010) 1059–1069.
[12] Z. Yang, S.V. Garimella, Thermal analysis of solar thermal energy storage in a molten-salt thermocline, Solar Energy 84 (2010) 974–985.
[13] C. Xu, Z. Wang, Y. He, X. Li, F. Bai, Sensitivity analysis of the numerical study on the thermal performance of a packed-bed molten salt thermocline thermal storage system, Appl. Energy 92 (2012) 65–75.
[14] A. Bruch, J.F. Fourmigué, R. Couturier, S. Molina, Experimental and numerical investigation of stability of packed bed thermal energy storage for CSP power plant, Energy Procedia 49 (2014) 743–751.
[15] N. Mertens, F. Alobaid, L. Frigge, B. Epple, Dynamic simulation of integrated rock-bed thermocline storage for concentrated solar power, Solar Energy 110 (2014) 830–842.
[16] Z. Yang, S.V. Garimella, Cyclic operation of molten-salt thermal energy storage in thermoclines for solar power plants, Appl. Energy 103 (2013) 256–265.
[17] S.M. Flueckiger, S.V. Garimella, Second-law analysis of molten-salt thermal energy storage in thermoclines, Solar Energy 86 (2012) 1621–1631.
[18] S. Flueckiger, Z. Yang, S.V. Garimella, An integrated thermal and mechanical investigation of molten-salt thermocline energy storage, Appl. Energy 88 (2011) 2098–2105.
[19] C. Mira-Hernández, S.M. Flueckiger, S.V. Garimella, Numerical simulation of single and dual-media thermocline tanks for energy storage in concentrating solar power plants, Energy Procedia 49 (2014) 916–926.
[20] Z. Yang, S.V. Garimella, Molten-salt thermal energy storage in thermoclines under different environmental boundary conditions, Appl. Energy 87 (2010) 3322–3329.
[21] A. Bruch, J.F. Fourmigué, R. Couturier, Experimental and numerical investigation of a pilot-scale thermal oil packed bed thermal storage system for CSP power plant, Solar Energy 105 (2014) 116–125.
[22] C. Xu, X. Li, Z. Wang, Y. He, F. Bai, Effects of solid particle properties on the thermal performance of a packed-bed molten-salt thermocline thermal storage system, Appl. Therm. Eng. 57 (2013) 69–80.
[23] K.M. Powell, T.F. Edgar, An adaptive-grid model for dynamic simulation of thermocline thermal energy storage systems, Energy Convers. Manag. 76 (2013) 865–873.
[24] R. Bayón, E. Rojas, Simulation of thermocline storage for solar thermal power plants: from dimensionless results to prototypes and real-size tanks, Int. J. Heat Mass Transf. 60 (2013) 713–721.
[25] J.T. Van Lew, P. Li, C.L. Chan, W. Karaki, J. Stephens, Analysis of Heat Storage and Delivery of a Thermocline Tank Having Solid Filler Material, J. Solar Energy Eng. 133 (2011) 1–10.
[26] P. Li, J. Van Lew, C. Chan, W. Karaki, J. Stephens, J.E. O'Brien, Similarity and generalized analysis of efficiencies of thermal energy storage systems, Renew. Energy 39 (2012) 388–402.
[27] R. Bayón, E. Rojas, Analytical function describing the behaviour of a thermocline storage tank: a requirement for annual simulations of solar thermal power plants, Int. J. Heat Mass Transf. 68 (2014) 641–648.
[28] D. McDonnell, 10 MWe solar thermal central receiver pilot plant, mode 5 (test 1150) and mode 6 (test 1160), test report, *SAND86-8175*, 1986.
[29] S. Flueckiger, B. Iverson, S.V. Garimella, J.E. Pacheco, System-level simulation of a solar power tower plant with thermocline thermal energy storage, Appl. Energy 113 (2014) 86–96.
[30] K.A.R. Ismail, R. Stuginsky Jr., A parametric study on possible fixed bed models for pcm and sensible heat storage, Appl. Therm. Eng. 19 (1999) 757–788.
[31] S.E. Faas, L.R. Thorne, E.A. Fuchs, N.D. Gilbertsen, 10 MWe solar thermal central receiver pilot plant: thermal storage subsystem evaluation – final report, *SAND86-8212*, 1986.
[32] A. Modi, C. Pérez-Segarra, Thermocline thermal energy storage systems for concentrated solar power plants: one-dimensional numerical model and comparative analysis, Solar Energy 100 (2014) 84–93.
[33] S. Flueckiger, Z. Yang, S.V. Garimella, Thermocline energy storage in the Solar One power plant: an experimentally validated thermo mechanical investigation, *Proceedings ASME ES2011*, 2011, 1–8.
[34] R.W. Carling, L.G. Radosevich, Specific heat variations in oil energy storage media and their economic implications, Solar Energy 22 (1979) 471–475.